Electrochimica Acta 246 (2017) 757–765

Contents lists available at ScienceDirect

Electrochimica Acta

journal homepage: www.elsevier.com/locate/electacta

Intense pulsed white light assisted fabrication of Co-CoOx core-shell nanoflakes on graphite felt for flexible hybrid supercapacitors

Changyong Park[a], Jeonguk Hwang[a], Yeon-Taek Hwang[b], Chiho Song[a], Suhyun Ahn[a], Hak-Sung Kim[b,c], Heejoon Ahn[a,c,*]

[a] Department of Organic and Nano Engineering, Hanyang University, Seoul, 04763, South Korea
[b] Department of Mechanical Engineering, Hanyang University, Seoul 04763, South Korea
[c] Institute of Nano Science and Technology, Hanyang University, Seoul 04763, South Korea

ARTICLE INFO

Article history:
Received 31 January 2017
Received in revised form 15 June 2017
Available online 17 June 2017

Keywords:
Intense pulsed white light
hybrid supercapacitor
nanostructure
energy storage
cobalt oxide

ABSTRACT

In this work, cobalt/cobalt oxide (Co-CoOx) core-shell nanoflakes were directly grown on flexible graphite felt (GF) using a facile one-step intense pulsed white light (IPWL) irradiation method. They were then used as a battery-type positive electrode for a high-performance asymmetric hybrid supercapacitor, which exhibited high rate capability and a long cycle life. The interconnected Co-CoOx thin nanoflakes grown on the GF offer large reaction sites and enough space for easy OH^- ion transport due to their 3-dimensionally interconnected network structures. Cobalt metal at the core of the nanoflakes, directly connected to the current collector of the GF, provided pathways for electrons between the cobalt oxide and GF, leading to low internal resistance and high rate capability. The Co-CoOx/GF electrode had a high specific capacity of 108 mAh g^{-1} at a specific current of 1 A g^{-1} and maintained a capacity of 71 mAh g^{-1} at a high specific current of 20 A g^{-1}. A two-terminal asymmetric hybrid supercapacitor, assembled using Co-CoOx/GF as the positive electrode and activated carbon as the negative electrode with gel-electrolyte (PVA/KOH), exhibited an energy density of 30.1 Wh kg^{-1} at a power density of 0.86 kW kg^{-1} and a high retention of 13.0 Wh kg^{-1} at a power density of 20.4 kW kg^{-1}. In addition, the asymmetric device showed excellent cycling stability, with 114% capacity retention after 10,000 cycles.

1. Introduction

Because interest in flexible electronics is increasing, many researchers in recent years have made efforts to develop flexible and bendable energy storage devices [1–5]. In general, energy storage devices consist of three key components: a current collector, an active material, and a separator/electrolyte [1]. For flexible energy storage devices, these components should be able to perform appropriately under mechanical bending strain. Among the components, the current collector significantly influences the performance of flexible devices because it occupies a substantial part of the device and because the mechanical strength and electrical properties of the flexible device mostly depend on the mechanical and electrical properties of the current collector [6]. Therefore, in designing flexible and bendable energy storage systems, selection of suitable current collectors and supporting substrates is important. Recently, graphite felt (GF) [7], carbon cloth [8,9], and carbon textiles [10,11] have been investigated as current collectors for flexible electrodes. Among them, GF is an excellent supporting substrate/current collector due to its reasonable electrical conductivity, high electrochemical stability, and high porosity and mechanical flexibility [7,12].

Supercapacitors have greater cycle stability and faster charge-discharge time than Li-ion batteries, but their energy density is poorer [13–15]. The energy density of a supercapacitor is determined by the specific capacitance and operating voltage, indicating two possible approaches for improvement: expanding the operating cell voltage and increasing the capacitance [16–18]. Electrical double-layer capacitors (EDLCs) that are based on carbon materials can achieve higher capacitance in aqueous electrolytes than in organic electrolytes, but they operate in a limited potential range (<1 V) in aqueous electrolytes due to water decomposition [14,18–22]. One efficient way to improve the energy of an aqueous electrolyte-based supercapacitor is to design a hybrid system composed of a faradaic non-capacitive battery-type positive electrode and a non-faradaic capacitive EDLC-type negative electrode. The energy density of the hybrid system can then be

* Corresponding authors at: Department of Organic and Nano Engineering, Hanyang University, Seoul, 04763, South Korea.
E-mail address: ahn@hanyang.ac.kr (H. Ahn).

http://dx.doi.org/10.1016/j.electacta.2017.06.087
0013-4686/

enhanced because the battery-type materials, such as metal hydroxides ($Ni(OH)_2$, $Co(OH)_2$) [23,24] and metal oxides ($NiCo_2O_4$, NiO, Co_3O_4, CoO) [25–28], have a high theoretical capacity based on faradaic redox reactions via transitions between multiple oxidation states. However, metal hydroxide- and oxide-based energy storage devices have limited power density because of their low electronic conductivity [29–31]. This phenomenon becomes more conspicuous when these materials are applied to carbon-based flexible substrates such as GF, carbon cloth, and carbon textiles because of their lower electrical conductivity compared with conventional metal current collectors such as Ni foams, stainless steel, and Al foil. One efficient way to improve the rate capability of battery-type positive electrodes is to design hierarchical structures for the electrode materials for easy charge diffusion and transfer [32–35]. Another way to improve the rate capability of the electrode is to increase the electrical conductivity of the electrode materials by designing metal/metal oxide (or hydroxide) core-shell-type hetero-structures. With a core-shell structure, the electrically conductive metal core can facilitate the transport of electrons between the current collector and the shell of the metal oxide (or hydroxide), which can result in enhanced rate capability and power for metal hydroxide- and oxide-based energy storage devices. In addition, because the conductivity of electrode materials greatly influences the electrochemical properties, highly conductive materials show low polarization, which results in high utilization of the active materials and enhanced electrochemical performance. Therefore, growing metal/metal oxide core-shell electrodes directly on carbon-based flexible substrates can create high-performance flexible and bendable energy storage devices.

Another issue in metal hydroxide- and oxide-based energy storage devices is the synthesis of nanostructured metal oxides/hydroxides. 3D-nanostructured metal hydroxides/oxides have been synthesized using various methods, including hydrothermal [26–28,36], microwave [37,38], chemical precipitation [39], and solution methods [40]. Typically, those methods require high annealing temperatures and long reaction times to convert metal-precursors into metal oxides. In addition, when metal oxides need to be incorporated with conductive materials, the method involves multiple steps. Therefore, facile, fast, energy-efficient methods for metal oxide/hydroxide 3D-nanostructure production are of interest.

In this study, we report an extremely facile approach to fabricating binder-free 3D-nanostructured cobalt oxide (CoOx) incorporated with conductive Co metal (Co) on a flexible current collector using a simple one-step intense pulsed white light (IPWL) technique. IPWL irradiation transfers heat energy in the form of light from a xenon lamp that emits a light spectrum in the visible region [41]. Cobalt metal/cobalt oxide (Co-CoOx) core-shell nanoflakes are fabricated on GF by irradiating $Co(NO_3)_2$-coated GF substrate with IPWL for a few milliseconds under atmospheric pressure at room temperature. The Co-CoOx core-shell nanoflakes on GF exhibit high rate capability and excellent cycling stability. The interconnected Co-CoOx nanoflakes offer many electroactive sites for faradaic reactions with electrolyte and porous spaces for easy ion/charge diffusion. In addition, the incorporated cobalt metal, which connects the active CoOx to the current collector in the GF, facilitates electron transfer between the CoOx and GF and minimizes the internal resistance of the electrode, resulting in high electrochemical performance. In addition, Co contributes to the structural stability of the electrode during cycles.

2. Experimental

2.1. Preparation of Co-CoOx nanoflakes on GF by IPWL irradiation

Prior to IPWL irradiation, the GF substrate was electrochemically oxidized by applying a constant potential of 2 V for 90 s in an aqueous solution of 0.5 M H_2SO_4 using a CHI 660D electrochemical workstation (CH Instrument) to improve the wettability of the GF to the metal oxide precursor solution. The GF substrate was washed with acetone and deionized (DI) water several times and dried at 60 °C for 6 hr. After that, the GF substrate was soaked in 0.4 M $Co(NO_3)_2 \bullet 6H_2O$ aqueous solution for 10 min. After drying in a vacuum at 50 °C for 2 h, the metal oxide precursor-coated GF was irradiated under IPWL at a total energy of 30 J cm^{-2} with two pulses (10 ms on time and 30 ms off time) at room temperature in ambient conditions. The distance between the sample and xenon lamp was a few millimeters. After irradiation, the samples were washed with DI water several times to remove residue and dried in an oven at 60 °C. The mass loading of CoOx-Co was about 0.8 mg and the thickness of the as-prepared electrode including GF was 0.9 mm. The mass of GF (1×2 cm^2) was 14 mg.

2.2. Preparation of activated carbon (AC) electrodes

The negative electrodes for the asymmetric hybrid supercapacitor were prepared by mixing AC (MSC-30, Kansai Coke & Chemicals Co. Ltd.), poly(vinylidene fluoride) (M.W. 534,000, Sigma-Aldrich), and carbon black (Super P, TIMCAL Graphite & Carbon) in a weight ratio of 8:1:1. A small amount of N-methyl-2-pyrrolidone (Sigma-Aldrich) was added to form a slurry. A doctor blade was used to cast the carbon slurry on graphite foil. Then, the coated electrodes were dried at 90 °C for 3 h to remove all solvents.

2.3. Integration of asymmetric hybrid supercapacitors

An asymmetric hybrid supercapacitor was constructed by sandwiching the Co-CoOx/GF (positive electrode) and the AC (negative electrode) with a PVA/KOH gel-electrolyte. The gel-electrolyte was fabricated by mixing 8 g of poly(vinyl alcohol) (PVA, M.W. 89,000-98,000) and 4 g KOH in 60 mL of DI water under vigorous stirring at 80 °C for 1 h. The gel-electrolyte was spread over the electrodes using a glass rod. Then, the gel-electrolyte-coated electrodes were put under vacuum for 5 min at 40 °C to remove air bubbles. After that, the gel electrolyte-coated electrodes were solidified for 6 h at room temperature. The size of each electrode was 1×2 cm^2 and the total thickness of an asymmetric hybrid supercapacitor was 1.15 mm.

2.4. Material characterization

The structure and morphology of the fabricated samples were studied using field-emission scanning electron microscopy (FE-SEM, S-4800, Hitachi) and field-emission transmission electron microscopy (FE-TEM, JEM-2100F, JEOL). To analyze the crystal structures, X-ray diffraction (XRD, D8 Advance, Bruker) measurements were examined with monochromatized Cu-Kα radiation. The volume fractions of the crystals appearing in the samples were estimated by calculating the area of a main peak of each crystal which was fitted by using a Gaussian function. The pore structure and Brunauer-Emmett-Teller (BET) surface area were measured using an Autosorb-iQ 2ST/MP (Quantachrome) analyzer at 77.35 K.

2.5. Electrical conductivity measurement

The electrical conductivity of the GF and Co-CoOx/GF was measured using a four-probe conductivity measurement system

(M4P-205, MSTECH). The measured electrical conductivity of the GF and Co-CoOx/GF are 45.9 S cm^{-1} and 21.2 S cm^{-1}, respectively.

2.6. Electrochemical measurement

All of the electrochemical tests were carried out using a CHI 660D electrochemical workstation at room temperature. To create a standard three-electrode system, the as-prepared Co-CoOx/GF or AC single electrode was directly used as the working electrode, Hg/HgO (CH Instrument) as the reference electrode, and coiled Pt wire (MW-1033, BASi) as the counter electrode. The electrochemical properties of the asymmetric hybrid supercapacitor were measured using a two-electrode system, with the AC electrode as the negative electrode and the Co-CoOx/GF electrode as the positive electrode. The optimal mass ratio of the negative electrode to the positive electrode was decided based on charge balance theory, as reflected in equations (1) and (2) [42,43]:

$$q^+ = q^- \quad (1)$$

$$q = C_S \times \Delta V \times m \quad (2)$$

where q (C) is the amount of charge stored, ΔV is the width of the operating potential window, C_S (F g^{-1}) is the specific capacitance of the electrode, and m (g) is the mass of the active materials. However, it is known that cobalt oxides behave like a battery-type material in non-capacitive faradaic reactions [22,44]. Thus, to describe the electrochemical behavior of these battery-type materials, the specific capacity (mAh g^{-1} or C g^{-1}) is used instead of the specific capacitance (F g^{-1}) [22]. Therefore, the charge stored at the positive electrode (Co-CoOx/GF) can be calculated using equation (3):

$$q^+ = Q_{S,+} \times m_+ \times 3.6 \quad (3)$$

where $Q_{S,+}$ (mAh g^{-1}) is the specific capacity of the positive electrode, and m_+ (g) is the mass of the active materials (Co-CoOx) in the positive electrode. The active electrode masses of the Co-CoOx/GF and AC were balanced based on the charges passed across the negative and positive electrodes ($q^+ = q^-$) according to equation (4):

$$\frac{m_+}{m_-} = \frac{C_{S,-} \times \Delta V_-}{Q_{S,+} \times 3.6} \quad (4)$$

where $C_{S,-}$ (F g^{-1}) is the specific capacitance of the negative electrode, and ΔV_- is the operating potential window for the negative electrode. Based on this equation, an optimal mass ratio (m_+/m_-) of 0.95 was calculated.

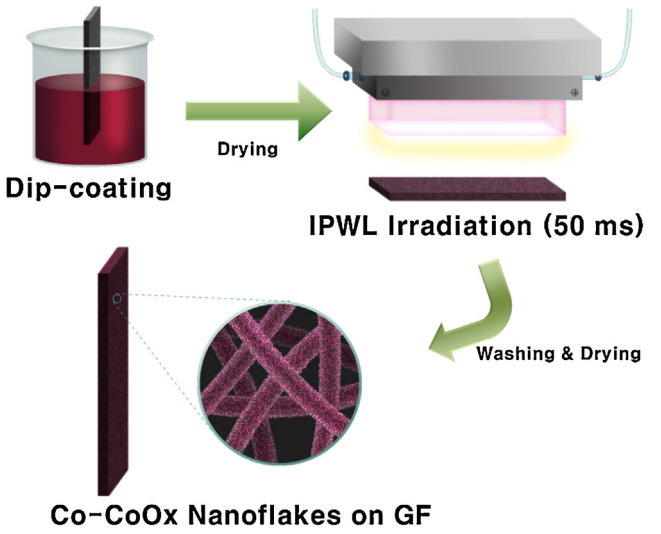

Scheme 1. Schematic illustration of the facile fabrication process of the Co-CoOx/GF electrode.

3. Results and discussion

The fabrication process of the Co-CoOx/GF electrode is schematically illustrated in Scheme 1. The Co-CoOx nanostructures can easily be fabricated on the flexible current collector (GF) by irradiating the precursor-coated GF substrate with IPWL for 50 ms. The mechanism for the formation of the Co-CoOx by IPWL irradiation is the thermal conversion of $Co(NO_3)_2$ to CoOx and further reduction to Co by IPWL irradiation. Recently, we have reported that the temperature of the $CoCl_2$-coated Ni-foam

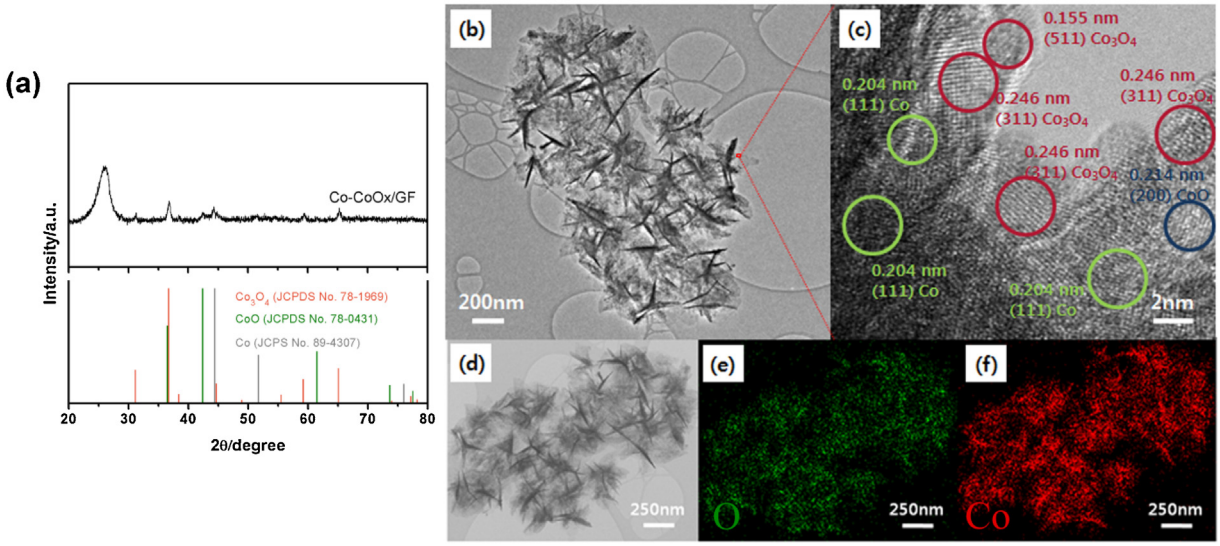

Fig. 1. (a) XRD spectrum of the Co-CoOx/GF electrode after IPWL irradiation with an energy density of 30 J cm^{-2}. (b) FE-TEM image of Co-CoOx nanoflakes. (c) High-resolution FE-TEM image of the edge of a nanoflake. (d) STEM image of Co-CoOx nanoflakes and (e and f) the corresponding elemental mapping images.

substrate can be increased up to 500 °C by IPWL irradiation because the IPWL irradiation transfers the heat energy in the form of light [45]. Thus, for the formation of the Co-CoOx, the $Co(NO_3)_2$ on GF is converted to CoOx and further reduced to Co by IPWL irradiation. Particularly, the reduction of CoOx to Co in this process is based on a carbothermal reaction [46]. The GF substrate is used as a reducing agent. This can explain the formation of the Co-CoOx core-shell structure on the GF substrates. During IPWL irradiation, the $Co(NO_3)_2$ is converted into CoOx nanoflakes, and the core part of the CoOx nanoflakes, which is either very close to the GF substrate or in direct contact with the GF substrate, is further reduced to Co by IPWL irradiation. However, the shell part of the CoOx nanoflakes, which is apart from the GF substrate and exposed to the air, is remained as CoOx. The content of CoOx and Co can be controlled by adjusting the energy of the IPWL irradiation. Increasing the energy of IPWL irradiation will increase the temperature of the samples. Higher irradiation energy (higher sample temperature) reduce Co_3O_4 to CoO and further to Co. So, as the irradiation energy is increased, the relative content of Co compared to CoOx is increased.

The crystallinity and morphology of the samples fabricated by IPWL irradiation were analyzed using XRD, FE-TEM, and FE-SEM. Fig. 1a shows the XRD spectrum of the Co-CoOx/GF electrode fabricated by IPWL irradiation with an energy density of 30 J cm^{-2}. As seen in the XRD pattern, Co and CoOx formed on the GF after IPWL irradiation. The peaks at 31.3, 36.8, 44.8, 59.4, and 65.2° are assignable to the (220), (311), (400), (511), and (440) planes of face-centered-cubic (FCC) Co_3O_4 (JCPDS card No. 78-1969), respectively. The peaks at 42.4 and 61.5° correspond to the (200) and (220) planes of FCC CoO (JCPDS card No. 78-0431), respectively, and those at 44.2 and 51.5° correspond to the (111) and (200) planes of FCC metallic Co (JCPDS card No. 89-4307). The volume fraction of the Co_3O_4, CoO and Co are calculated to be 63.8%, 20.3%, and 15.9%, respectively. Energy dispersive X-ray spectroscopy elemental mapping images (Fig. 1e and f) show that Co and O are homogeneously distributed all over the Co-CoOx nanoflake structures. The morphology and crystallinity of the samples were further analyzed using high-resolution TEM. As shown in Fig. 1b, a TEM image of the Co-CoOx sample shows the formation of network-like structures of interconnected nanoflakes. The size of the nanoflake structures is 200–400 nm, and the thickness is less than 50 nm. Fig. 1c shows a high-resolution TEM image of the edge of a nanoflake. Inter-planar lattice distances of 0.246, 0.155, 0.214, and 0.204 nm in the sample correspond to the (311) and (511) planes of FCC Co_3O_4, the (200) plane of FCC CoO, and the (111) plane of FCC metallic Co, respectively. As shown in the figure, the metallic Co core is covered with a thin layer of Co_3O_4, which confirms that the Co-CoOx nanoflakes are composed of a metallic Co core surrounded by a Co_3O_4 and CoO sheath layer. The core-shell structure of Co-CoOx can be further confirmed by the high-resolution elemental mapping images of the Co-CoOx nanoflake. As shown in Fig. S1, the O element is evenly distributed on the

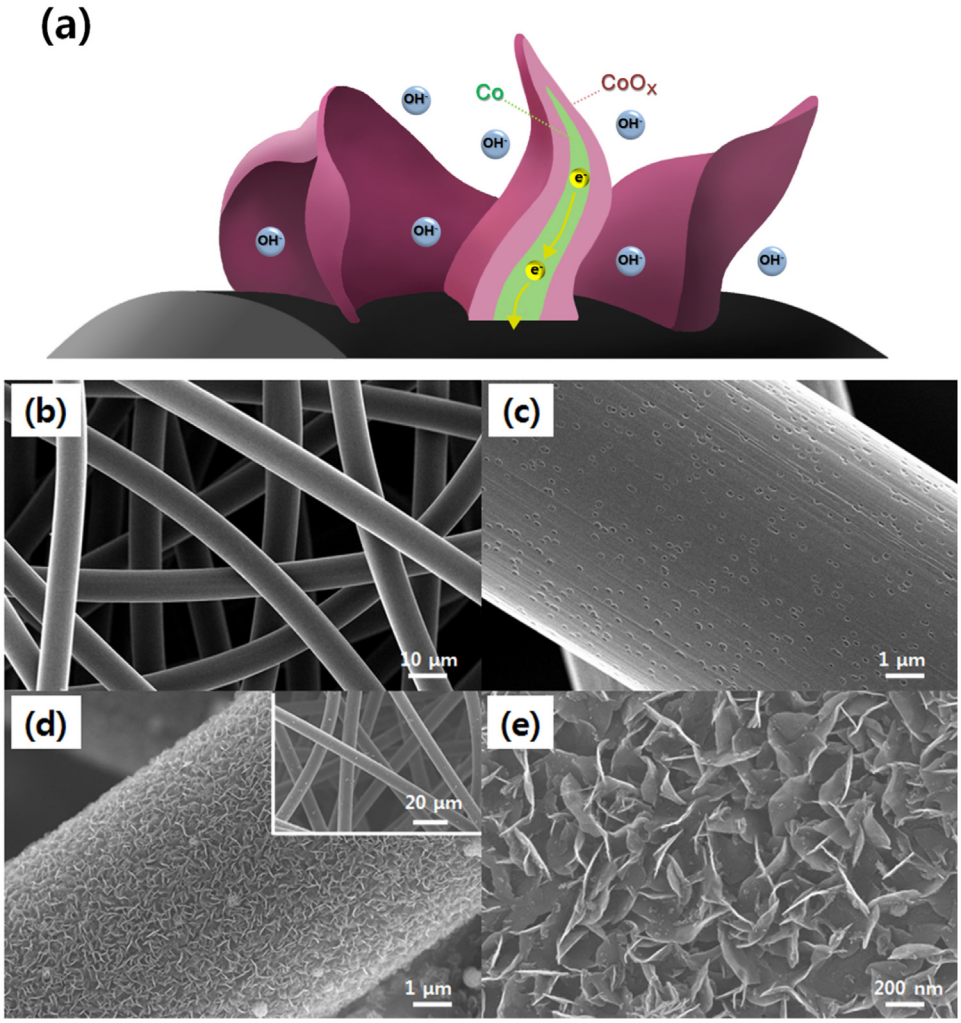

Fig. 2. (a) Schematic illustration of Co-CoOx nanoflakes on GF. FE-SEM images of oxidized GF (b and c) and Co-CoOx/GF electrodes (d and e).

surface of nanoflakes. Unlike the O element, Co element is more concentrated in the core compared to the shell. These results also display the Co-CoOx core-shell structures. As illustrated in Fig. 2a, the metallic cobalt at the core of the nanoflakes forms a bridge between the CoOx and the GF current collector, facilitating electron transfer from the surface of the active material to the current collector during faradaic reactions, which ensures the high electrochemical performance of CoOx under high-rate charge/discharge conditions.

Fig. 2b and c show SEM images of acid-treated GF composed of carbon fibers with an average diameter of 8 μm. Fig. 2d and e are SEM images of Co-CoOx/GF after IPWL irradiation. As seen in the figure, porous structures of inter-connected Co-CoOx nanoflakes uniformly coat the surface of the carbon fibers. Interconnected nanoflakes grow almost vertically directly on the surface carbon fibers. Thin nanoflakes provide a large surface area in the electrode, and the interconnected nanoflake structures contribute to the porosity of the electrode. The porosity of the GF and Co-CoOx/GF electrodes was further characterized by using nitrogen adsorption-desorption isotherms (Fig. S2a). The BET surface area of GF and Co-CoOx/GF were 5.84 $m^2 g^{-1}$ and 106.17 $m^2 g^{-1}$, respectively. The BET surface area of Co-CoOx/GF is much higher than that of the GF because of the inter-connected Co-CoOx nanoflakes on the GF substrate. The pore size distributions of the samples were measured using the Barrett-Joyner-Halenda (BJH) method (Fig. S2b). In case of Co-CoOx/GF electrode, the majority of pores are in the mesoporous region (> 3 nm). The large surface area and porous structures provide large reaction sites and easy electrochemical accessibility for electrolyte ions, ensuring the high capacity and rate capability of the electrode.

Electrochemical properties of Co-CoOx/GF electrodes were investigated using a standard three-electrode system. The cyclic voltammetry (CV) and galvanostatic charge-discharge (GCD) measurements of the Co-CoOx/GF electrodes were carried out in 1 M KOH aqueous electrolyte with a potential window of 0 to 0.55 V (vs. Hg/HgO). Fig. 3a shows the CV curves of the Co-CoOx/GF electrode at scan rates from 10 to 100 mV s^{-1}. The inset shows the CV curve of the Co-CoOx/GF electrode at a scan rate of 5 mV s^{-1}. The non-rectangular shape of the CV curves indicates that non-capacitive faradaic reactions are responsible for charge storage in the Co-CoOx/GF at potential ranges from 0 to 0.55 V. Thus, the specific capacity (mAh g^{-1} or C g^{-1}) is calculated instead of the specific capacitance (F g^{-1}). The mass loading of CoOx-Co was 0.812 mg. The redox peaks on the CV curves originate from the reversible faradaic charge storage processes in the alkaline electrolyte associated with the reactions shown in (5), (6), and (7) [47–50]:

$$Co_3O_4 + OH^- + H_2O \leftrightarrow 3CoOOH + e^- \quad (5)$$

$$CoOOH + OH^- \leftrightarrow CoO_2 + H_2O + e^- \quad (6)$$

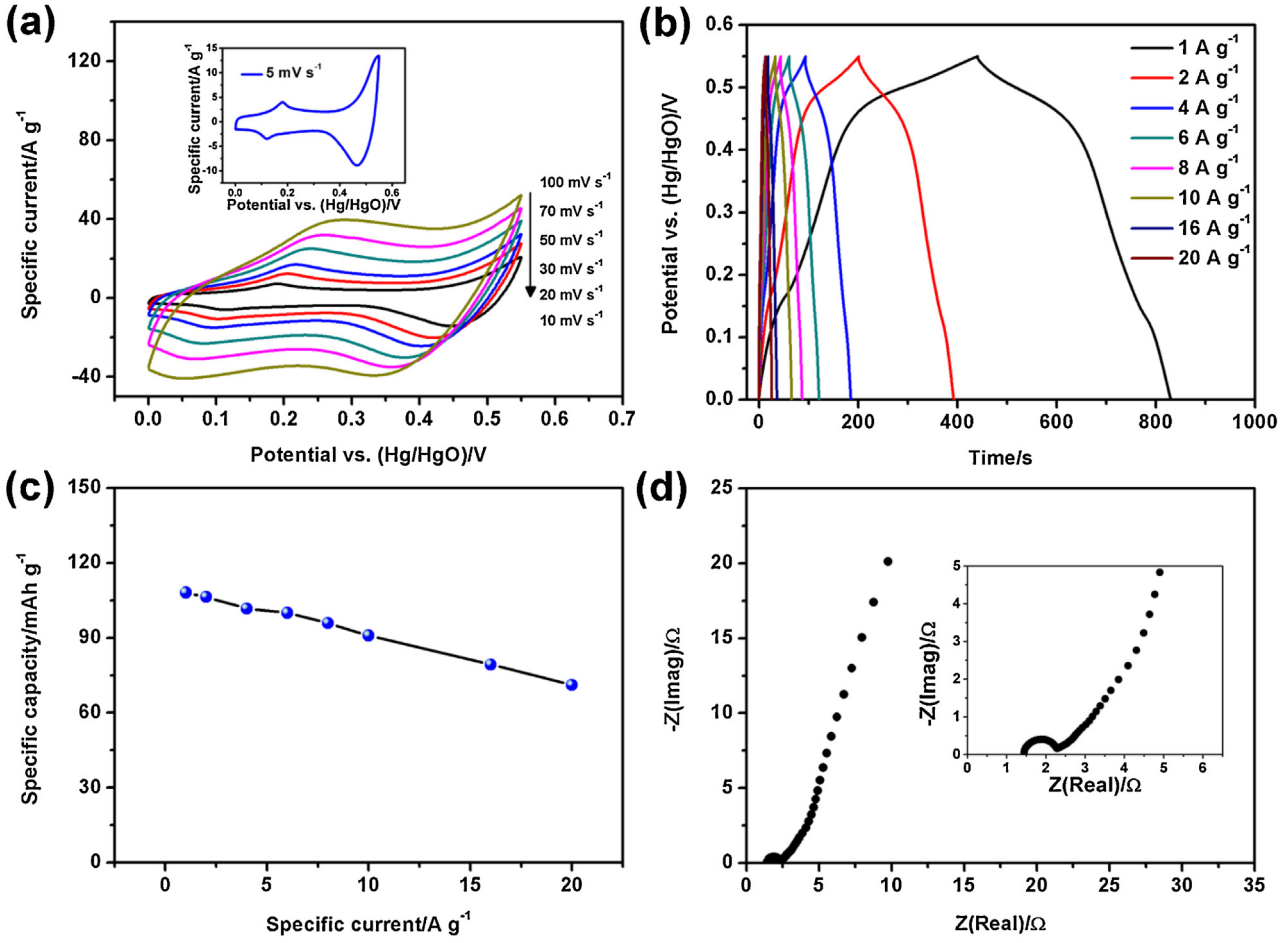

Fig. 3. (a) CV curves of a Co-CoOx/GF electrode in a three-electrode cell with 1 M KOH aqueous solution at scan rates from 10 to 100 mV s^{-1}; the inset shows the CV curve at a scan rate of 5 mV s^{-1}. (b) GCD curves of a Co-CoOx/GF electrode at various specific currents. (c) Specific capacity of a Co-CoOx/GF electrode as a function of specific current. (d) Nyquist plot of a Co-CoOx/GF electrode.

$$CoO + 2OH^- \leftrightarrow CoO_2 + H_2O + 2e^- \quad (7)$$

The theoretical capacities of Co_3O_4 and CoO, calculated based on those reactions, are 445 mAh g^{-1}(1603 C g^{-1}) and 715 mAh g^{-1} (2575 C g^{-1}), respectively. Small potential separation between the oxidation and reduction peaks indicates that reversible redox reactions occur at the CoOx shell of the nanoflakes [51]. Fig. 3b shows the GCD curves of a Co-CoOx/GF electrode at various specific currents from 1 to 20 A g^{-1}. As shown in the figure, the slopes of the GCD curves are unlike the triangular shape typically seen in EDLC-type electrodes, indicating that the Co-CoOx/GF electrode behaves as a battery-type non-capacitive material. This is consistent with the results of the CV measurements. The specific capacity ($Q_{S,+}$ in mAh g^{-1}) of the Co-CoOx/GF electrode is obtained from the GCD curve using equation (8):

$$Q_{S,+} = \frac{I \times \Delta t}{3.6 \times m_+} \quad (8)$$

where I (A) is the discharge current, Δt (s) is the discharge time, and m_+ (g) is the mass loading of active material (including Co and CoOx). Fig. 3c shows the specific capacity of the Co-CoOx/GF electrode as a function of specific current. The Co-CoOx/GF electrode exhibits a high specific capacity of 108 mAh g^{-1} (389 C g^{-1}) at a specific current of 1 A g^{-1} (0.41 mA cm^{-2}). Moreover, the electrode shows a specific capacity of 71 mAh g^{-1} (256 C g^{-1}) at a

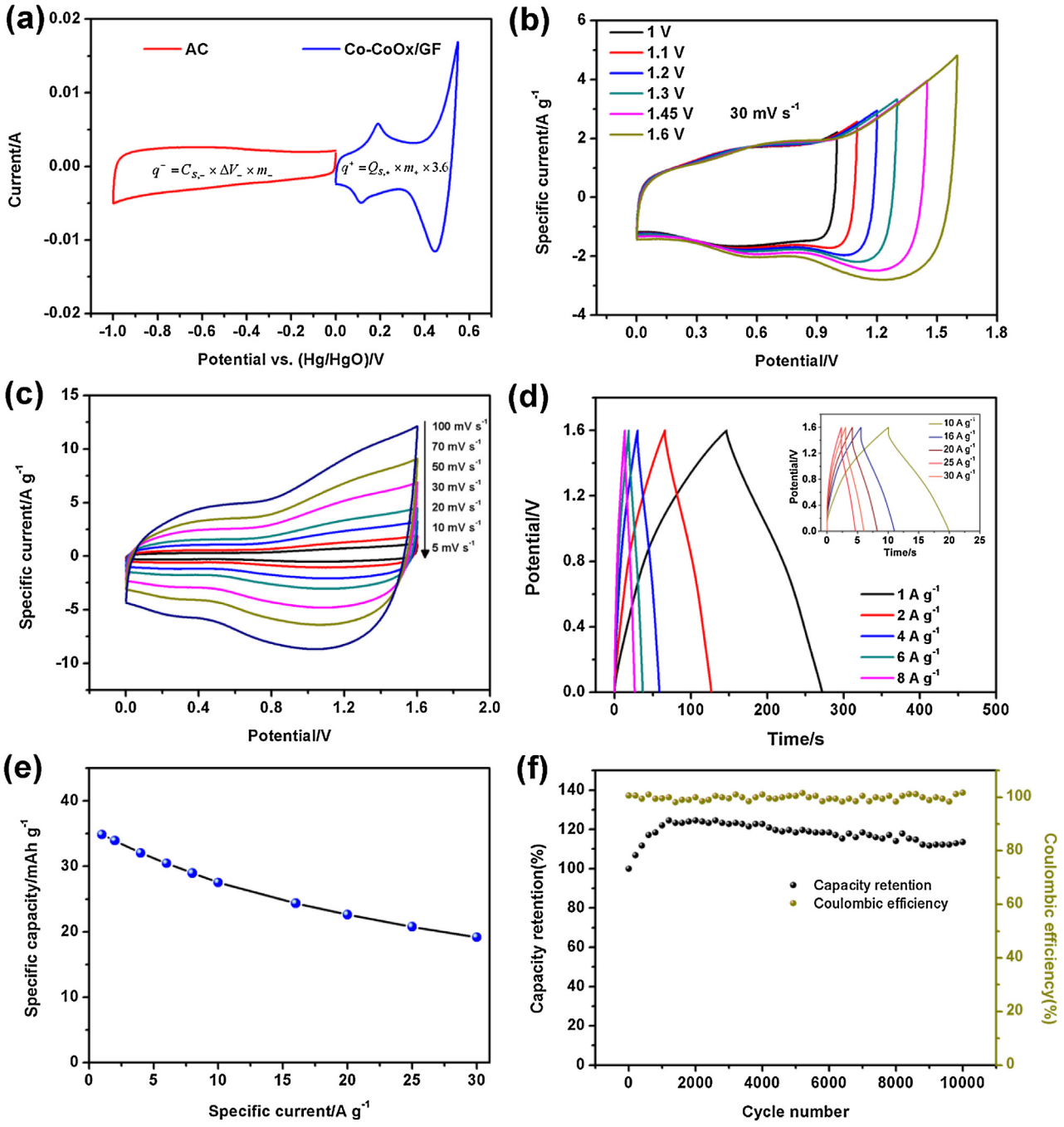

Fig. 4. (a) CV curves of negative and positive electrodes at 30 mV s^{-1}. (b) CV curves of a Co-CoOx/GF//AC ASC measured at different potential windows. (c) CV curves of a Co-CoOx/GF//AC ASC at scan rates from 5 to 100 mV s^{-1}. (d) GCD curves of a Co-CoOx/GF//AC ASC at various specific currents. (e) Specific capacity of a Co-CoOx/GF//AC ASC as a function of specific current. (f) Capacity retention and coulombic efficiency of a Co-CoOx/GF//AC ASC.

high specific current of 20 A g^{-1} (8.1 mA cm^{-2}), which is about 66% of the capacity at 1 A g^{-1}. This result suggests that the Co-CoOx/GF electrode has high rate capability, which is beneficial for high power delivery.

To further investigate the electrochemical properties of the electrodes, electrochemical impedance spectroscopy (EIS) was studied in the frequency range of 10^5 to 10^{-1} Hz with an open circuit potential of 0.06 V by applying an amplitude of 5 mV. The thickness of Co-CoOx/GF electrode was 0.9 mm. As shown in Fig. 3d, the impedance spectrum has two main sections, a linear part (Warburg) in the low-frequency regions and a semicircular region in the high-frequency ranges. The slope of the linear part in the low-frequency regions corresponds to the Warburg contribution, which reflects the diffusive resistance caused by the diffusion of redox species in the electrolyte. The quasi-linear line inclined at a 45° angle to the real axis represents the infinite Warburg diffusion caused by diffusion-controlled electrode kinetics in the low-frequency regions [52]. The semicircular curve observed in the higher-frequency region is related to the charge transfer process caused by faradaic reactions. The charge transfer resistance (R_{ct}) can be obtained from the diameter of the semicircle of the impedance spectrum, which is 0.84 Ω for the Co-CoOx/GF electrode. This small R_{ct} indicates excellent efficiency of OH^- ion exchange at the electrode-electrolyte interface [51], which is caused by the 3-dimensionally interconnected nanoflake structures that provide expeditious access routes for OH^- ions and the center-located Co that forms electron paths within the active material. Thus, Co-CoOx/GF electrodes have low internal resistance and achieve good rate capability.

Asymmetric supercapacitor (ASC) with battery-type positive electrode and carbon negative electrode that have well separated potential windows feature higher specific energy than conventional EDLCs because of high theoretical capacity of battery-type materials. Here, we constructed an ASC using a Co-CoOx/GF battery-type faradaic positive electrode and an AC capacitor-type negative electrode (denoted Co-CoOx/GF//AC). Before assembling the ASC, we performed CV measurements using a three-electrode system in 1 M KOH aqueous electrolyte to evaluate the electrochemical potential windows and quantify the amount of charge stored in the positive and negative electrodes. Fig. 4a shows the CVs of the Co-CoOx/GF and AC half-cell electrodes measured in the potential window between −1.0 V and 0.55 V (vs. Hg/HgO) in 1 M KOH aqueous electrolyte at a scan rate of 30 mV s^{-1}. As shown in the figure, the AC electrode exhibits a quasi-rectangular CV curve without redox peaks in the potential range from −1.0 V to 0 V, which is typical EDLC-type capacitive behavior. The Co-CoOx/GF electrode shows electrochemically stable non-capacitive faradaic behavior in the potential range from 0 to 0.55 V (vs. Hg/HgO). Because the operating voltage of the two-electrode cell is regarded as the sum of the potential range of the positive and negative electrodes, it was expected that the operating cell voltage would be extended to about 1.55 V when the AC and Co-CoOx/GF were assembled into an ASC as the negative electrode and positive electrode, respectively. Fig. 4b shows the CV curves of an ASC (Co-CoOx/GF//AC) in various potential windows (0–1 V to 0–1.6 V) at a scan rate of 30 mV s^{-1}. Note that the Co-CoOx/GF//AC ASC was constructed using a PVA/KOH gel-electrolyte. As seen in Fig. 4b, the CV curves exhibit a quasi-mirror-image current response on voltage reversal, and the operating potential window of the Co-CoOx/GF//AC ASC can be extended up to 1.6 V. Fig. 4c shows the CV curves of the Co-CoOx/GF//AC ASC at various scan rates from 5 to 100 mV s^{-1}. The shape of the CV curves denotes the charging and discharging characteristics of the device. As shown in the figure, the CV curves have two pairs of smooth, broad redox peaks that result from the combination of the capacitive charge storing characteristic of the negative electrode and the battery-type charge storing characteristic of the positive electrode. The shape of the CV curve is maintained well even at the high scan rate of 100 mV s^{-1}, suggesting the high rate capability desirable for high-power hybrid supercapacitors. To further evaluate the electrochemical performance of the Co-CoOx/GF//AC ASC, we performed GCD measurements at various specific currents, and the results are shown in Fig. 4d. Both the charge and discharge curves are almost symmetric but deviate slightly from the ideal linear line because the Co-CoOx/GF//AC ASC has a non-capacitive faradaic charge storing characteristic, which is consistent with the results of the CV measurements. The specific capacity of the Co-CoOx/GF//AC ASC is calculated using equation (9):

$$Q_S = \frac{I \times \Delta t}{3.6 \times m} \tag{9}$$

where Q_S (mAh g^{-1}) is the total specific capacity of the ASC, I (A) is the discharge current, Δt (s) is the total discharge time, and m (g) is the total mass of active materials in the two electrodes. The total combined active electrode mass (Co-CoOx and AC) of the asymmetric hybrid supercapacitor was 1.5 mg and the mass loading of CoOx-Co was 0.736 mg. The specific capacity of the Co-CoOx/GF//AC ASC is 35 mAh g^{-1} at a specific current of 1 A g^{-1} (0.76 mA cm^{-2}) and 28 mAh g^{-1} (~80% retention) at 10 A g^{-1} (7.6 mA cm^{-2}). The device delivers 19 mAh g^{-1} even at the very high specific current of 30 A g^{-1} (22.7 mA cm^{-2}), which is 54% of the maximum specific capacity at 1 A g^{-1}, indicating the device's high rate capability. As can be seen from Fig. 2a, the excellent electrochemical performance of the Co-CoOx/GF//AC ASC can be

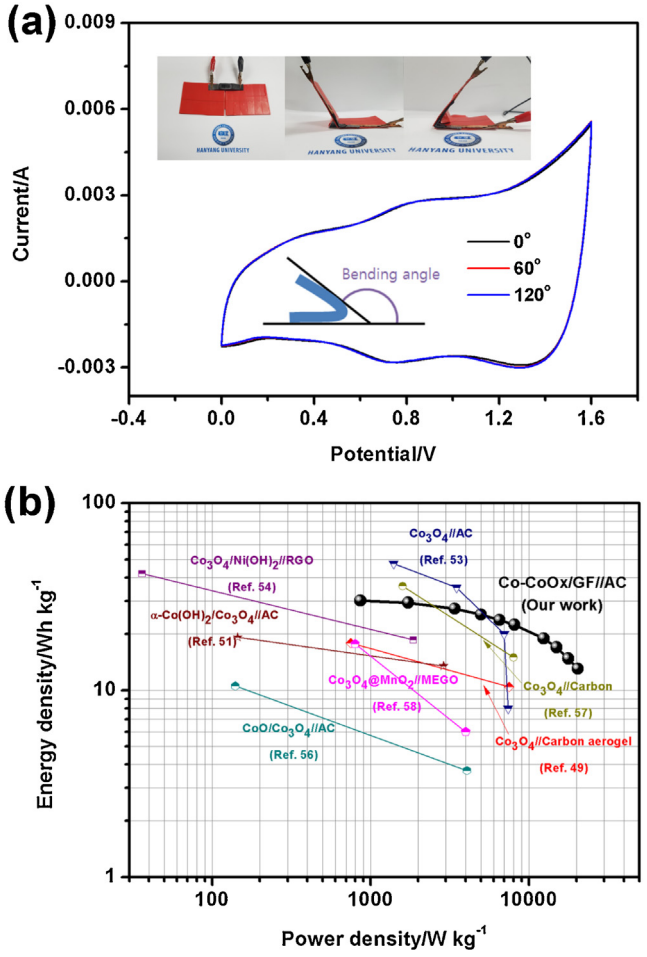

Fig. 5. (a) Bending test and (b) Ragone plot of a Co-CoOx/GF//AC ASC.

attributed to the following factors: (i) The Co-CoOx core-shell nanoflakes, which are grown directly on the flexible current collector without a binder, facilitate electron transfer at the interface between the active materials and the substrate; (ii) The porous 3D structure of the interconnected Co-CoOx nanoflakes provides large electroactive sites for redox faradaic reactions between the CoOx and the electrolyte and reduces the ion diffusion length, leading to easy ion transfer inside the electrode; (iii) The electrically conductive Co at the core of the nanoflakes forms a bridge between the CoOx and the GF current collector and facilitates electron transfer between them.

Cycling stability is an important characteristic of the energy storage system for practical applications. A cycle test of the as-prepared ASC was performed using the GCD method at a specific current of 10 A g^{-1} between 0 and 1.6 V for 10,000 cycles. As shown in Fig. 4f, the capacity increased during the initial 1,000 cycles and gradually degraded until 10,000 cycles. The initial enhancement of the capacity could result from infiltration of the gel electrolyte into the electrodes during charge/discharge cycles. The Co-CoOx/GF//AC ASC exhibits 114% retention of the specific capacity after 10,000 cycles compared with the initial value and shows 91% retention compared with the maximum specific capacity during the cycle. In addition, the device showed high coulombic efficiency (exceeding 98%) during the entire cycling test. The Co-CoOx/GF//AC ASC shows greater cycling stability than previously reported Co_3O_4-based asymmetric devices [49,51,53–55]. This excellent long-term cycle performance of the device is attributable to the presence of metallic Co at the core of the CoOx nanoflakes, which behaves as a mechanically stable frame in the electrode during the cycles. It is noteworthy that Co electrodes in alkaline electrolyte undergo a redox reaction at negative potentials below −0.282 V (vs. Hg/HgO) [50]. As seen from the XRD spectrum of the Co-CoOx/GF electrode after 100 cycles (see Fig. S3), there is no remarkable change from the XRD pattern of the Co-CoOx/GF electrode before the cycles. This result confirms that metallic Co still exists without any irreversible redox reactions in 1 M KOH aqueous electrolyte at a potential range from 0 to 0.55 V (vs. Hg/HgO). This inactive Co at the core of the nanoflakes not only creates electron paths between the GF and CoOx, but forms a structural support for the active materials that experience phase and volume changes during the cycles. Therefore, the Co-CoOx core-shell structure of the battery-type positive electrode allows this asymmetric device to achieve long-term cycle performance.

A supercapacitor's ability to mechanically flex or bend without losing electrochemical performance is of significant importance to the practical application of the device in flexible and bendable electronics. Thus, to investigate the mechanical flexibility and bendability of the Co-CoOx/GF//AC ASC, the CV measurements of the device were performed at different bending angles at a scan rate of 30 mV s^{-1} (Fig. 5a). As shown in the figure, the shapes of the CV curves remain the same at different bending angles, indicating the retention of capacitive performance up to a bending angle of 120°. This result also implies the excellent adhesion of the active electrode materials to the current collector (the Co-CoOx with GF and AC with GF) and the good quality of the interface between the PVA/KOH gel-electrolyte and the active electrode materials.

A Ragone plot, which shows the relation between the energy storage and power capabilities of energy storage devices, was used to evaluate the performance of the Co-CoOx/GF//AC ASC. The specific energy density and specific power density were calculated using equations (10) and (11), respectively:

$$E = \frac{I \times \int V dt}{3.6 \times m} \tag{10}$$

$$P = \frac{E}{\Delta t} \times 3600 \tag{11}$$

where E (Wh kg^{-1}) is the specific energy density, V (V) is the width of the operating potential, and P (W kg^{-1}) is the specific power density of the device. As seen in Fig. 5b, the Co-CoOx/GF//AC ASC exhibits an energy density of 30.1 Wh kg^{-1} (0.2 mWh cm^{-3}) at a power density of 0.86 kW kg^{-1} (5.6 mW cm^{-3}), with a high retention of 13.0 kW kg^{-1} (0.09 mWh cm^{-3}) at a power density of 20.4 kW kg^{-1} (133 mW cm^{-3}). The power performance of the device is comparable or superior to the performance previously reported for Co_3O_4-based asymmetric devices [49,51,53,54,56–58]. These results indicate that the Co-CoOx/GF//AC ASC, with its excellent energy/power delivery and cycling stability, holds great promise as an energy storage system.

4. Conclusions

In this study, we demonstrated an ultra-rapid and facile method to produce Co-CoOx core-shell nanostructures on a GF flexible current collector using a one-step IPWL technique. The IPWL-induced Co-CoOx/GF electrode exhibited the high specific capacity of 108 mAh g^{-1} at a specific current of 1 A g^{-1} and high rate capability, because of easy ion accessibility caused by the porous 3D structures of interconnected nanoflakes and the high electronic conductivity of the incorporated metallic Co at the core of the CoOx nanoflakes. The Co-CoOx/GF//AC ASC showed a specific energy of 30.1 Wh kg^{-1} at a specific power of 0.86 kW kg^{-1} and retained 43% of that energy density even at the specific power of 20.4 kW kg^{-1}. In addition, this hybrid supercapacitor exhibited excellent cycling stability (114% retention) over 10,000 cycles due to its unique Co-CoOx core-shell structure. The IPWL method can be readily applied to the production of other types of metal/metal oxide core-shell nanostructures on current collectors without the use of binder materials; therefore, this IPLW technology has great potential for energy storage systems.

Acknowledgments

This research was supported by a grant from the Technology Development Program for Strategic Core Materials funded by the Ministry of Trade, Industry, & Energy (10047758) and by grants from the Basic Science Research Program through the National Research Foundation of Korea (NRF) funded by the Ministry of Education (2012R1A6A1029029, 2014M3A7B4052201, and 2015R1A2A2A01008398), Republic of Korea. Authors thank to Sang-Hwa Lee and Prof. Jaeyong Kim from the Hanyang University for the calculation of the volume fractions of the crystals.

References

[1] K. Jost, G. Dion, Y. Gogotsi, Textile energy storage in perspective, J. Mater. Chem. A 2 (2014) 10776–10787.
[2] T. Chen, L. Dai, Flexible supercapacitors based on carbon nanomaterials, J. Mater. Chem. A 2 (2014) 10756–10775.
[3] H. Gwon, H.-S. Kim, K.U. Lee, D.-H. Seo, Y.C. Park, Y.-S. Lee, B.T. Ahn, K. Kang, Flexible energy storage devices based on graphene paper, Energy Environ. Sci. 4 (2011) 1277–1283.
[4] J. Bae, M.K. Song, Y.J. Park, J.M. Kim, M.L. Liu, Z.L. Wang, Fiber supercapacitors made of nanowire-fiber hybrid structures for wearable/flexible energy storage, Angew. Chem., Int. Ed. 50 (2011) 1683–1687.
[5] L. Hu, M. Pasta, F.L. Mantia, L. Cui, S. Jeong, H.D. Deshazer, J.W. Choi, S.M. Han, Y. Cui, Stretchable, porous, and conductive energy textiles, Nano Lett 10 (2011) 708–714.
[6] Y.-H. Lee, J.-S. Kim, J. Noh, I. Lee, H.J. Kim, S. Choi, J. Seo, S. Jeon, T.-S. Kim, J.-Y. Lee, J.W. Choi, Wearable textile battery rechargeable by solar energy, Nano Lett. 13 (2013) 5753–5761.

[7] M. He, Y. Zheng, Q. Du, Electrochemical fabrication of polyaniline/MnO_2/graphite felt as free-standing, flexible electrode for supercapacitors, Polym. Compos. 34 (2013) 819–824.
[8] Y.-K. Hsu, Y.-C. Chen, Y.-G. Lin, L.-C. Chen, K.-H. Chen, High-cell-voltage supercapacitor of carbon nanotube/carbon cloth operating in neutral aqueous solution, J. Mater. Chem. 22 (2012) 3383–3387.
[9] Z.-Y. Yu, L.-F. Chen, S.-H. Yu, Growth of NiFe2O4 nanoparticles on carbon cloth for high performance flexible supercapacitors, J. Mater. Chem. A 2 (2014) 10889–10894.
[10] B. Liu, X. Wang, H. Chen, Z. Wang, D. Chen, Y.-B. Cheng, C. Zhou, G. Shen, Hierarchical silicon nanowires-carbon textiles matrix as a binder-free anode for high-performance advanced lithium-ion batteries, Sci. Rep. 3 (2013) 1622–1628.
[11] L. Shen, B. Ding, P. Nie, G. Cao, X. Zhang, Advanced energy-storage architectures composed of spinel lithium metal oxide nanocrystal on carbon textiles, Adv. Energy Mater. 3 (2013) 1484–1489.
[12] B. Li, M. Gu, Z. Nie, Y. Shao, Q. Luo, X. Wei, X. Li, J. Xiao, C. Wang, V. Sprenkle, W. Wang, Bismuth nanoparticle decorating graphite felt as a high-performance electrode for an all-vanadium redox flow battery, Nano Lett. 13 (2013) 1330–1335.
[13] B.E. Conway, Electrochemical supercapacitor: scientific fundamentals and technological applications, Kluwer Academy, New York, 2009.
[14] P. Simon, Y. Gogotsi, Materials for electrochemical capacitors, Nat. Mater. 7 (2008) 845–854.
[15] J.R. Miller, P. Simon, Electrochemical capacitors for energy management, Science 321 (2008) 651–652.
[16] K. Fic, E. Frackowiak, F. Béguin, Unusual energy enhancement in carbon-based electrochemical capacitors, J. Mater. Chem. 22 (2012) 24213–24223.
[17] C. Arbizzani, M. Biso, D. Cericola, M. Lazzari, F. Soavi, M. Mastragostino, Safe, high-energy supercapacitors based on solvent-free ionic liquid electrolytes, J. Power Sources 185 (2008) 1575–1579.
[18] W.G. Pell, B.E. Conway, Peculiarities and requirements of asymmetric capacitor devices based on combination of capacitor and battery-type electrodes, J. Power Sources 136 (2004) 334–345.
[19] J. Menzel, K. Fic, E. Frackowiak, Hybrid aqueous capacitors with improved energy/power performance, Prog. Nat. Sci. 25 (2015) 642–649.
[20] A. Bruke, Ultracapacitors: why, how, and where is the technology, J. Power Sources 91 (2000) 37–50.
[21] J.P. Zheng, The limitations of energy density of battery/double-layer capacitor asymmetric cells, J. Electrochem. Soc. 150 (2003) A484–A492.
[22] T. Brousse, D. Bélanger, J.W. Long, To be or not to be pseudocapacitive? J. Electrochem. Soc. 162 (2015) A5185–A5189.
[23] F.-S. Cai, G.-Y. Zhang, J. Chen, X.-L. Gou, H.-K. Liu, S.-X. Dou, $Ni(OH)_2$ tubes with mesoscale dimensions as positive-electrode materials of alkaline rechargeable batterys, Angew. Chem. Int. Ed. 43 (2004) 4212–4216.
[24] R. Wang, X. Yan, J. Lang, Z. Zhengm, P. Zhang, A hybrid supercapacitor based on flower-like $Co(OH)_2$ and urchin-like VN electrode materials, J. Mater. Chem. A 2 (2014) 12724–12732.
[25] R.R. Salunkhe, K. Jang, H. Yu, S. Yu, T. Ganesh, S.-H. Han, H. Ahn, Chemical synthesis and electrochemical analysis of nickel cobaltite nanostructures for supercapacitor applications, J. Alloys Compd. 509 (2011) 6677–6682.
[26] J. Li, W. Zhao, F. Huang, A. Manivannan, N. Wu, Single-crystalline $Ni(OH)_2$ and NiO nanoplatelet arrays as supercapacitor electrode, Nanoscale 3 (2011) 5013–5019.
[27] S. Huang, Y. Jin, M. Jia, Preparation of graphene/Co_3O_4 composites by hydrothermal method and their electrochemical properties, Electrochim. Acta 95 (2013) 139–145.
[28] Y.G. Zhu, Y. Wang, Y. Shi, J.I. Wong, H.Y. Yang, CoO nanoflowers woven by CNT network for high energy density flexible micro-supercapacitor, Nano Energy 3 (2014) 46–54.
[29] S. Nandy, U.N. Maiti, C.K. Ghosh, K.K. Chattopadhyay, Enhanced p-type conductivity and band gap narrowing in heavily Al doped NiO thin films deposited by RF magnetron sputtering, J. Phys.: Condens, Matter 21 (2009) 115804–115810.
[30] M. Zhi, C. Xiang, J. Li, M. Li, N. Wu, Nanostructured carbon-metal oxide composite electrodes for supercapacitors: a review, Nanoscale 5 (2013) 72–88.
[31] Y. Wang, D. Zhou, D. Zhao, M. Hou, C. Wang, Y. Xia, High performance hybrid supercapacitor based on graphene-supported $Ni(OH)_2$-nanowires and ordered mesoporous carbon CMK-5, J. Electrochem. Soc. 160 (2013) A98–A104.
[32] Y. Xiao, S. Liu, F. Li, A. Zhang, J. Zhao, S. Fang, D. Jia, 3D hierarchical Co_3O_4 twin-spheres with an urchin-like structure: large-scale synthesis, multistep-splitting growth, and electrochemical pseudocapacitors, Adv. Funct. Mater. 22 (2012) 4052–4059.
[33] C. Yuan, X. Zhang, L. Su, B. Gao, L. Shen, Facile synthesis and self-assembly of hierarchical porous NiO nano/micro spherical superstructures for high performance supercapacitors, J. Mater. Chem. 19 (2009) 5772–5777.
[34] Q. Zhou, X. Wang, Y. Liu, Y. He, Y. Gao, J. Liu, High rate capabilities of $NiCo_2O_4$-based hierarchical superstructures for rechargeable charge storage, J. Electrochem. Soc. 161 (2014) A1922–A1926.
[35] H. Jiang, T. Zhao, C. Li, J. Ma, Hierarchical self-assembly of ultrathin nickel hydroxide nanoflakes for high-performance supercapacitors, J. Mater. Chem. 21 (2011) 3818–3823.
[36] L. Xie, K. Li, G. Sun, Z. Hu, C. Lv, J. Wang, C. Zhang, Preparation and electrochemical performance of the layered cobalt oxide (Co_3O_4) as supercapacitor electrode material, J.Solid State Electrochem. 17 (2013) 55–61.
[37] J. Yan, T. Wei, W. Qiao, B. Shao, Q. Zhao, L. Zhang, Z. Fan, Rapid microwave-assisted synthesis of graphene nanosheet/Co_3O_4 composite for supercapacitors, Electrochim. Acta 55 (2011) 6973–6978.
[38] S.K. Meher, G.R. Rao, Effect of microwave on the nanowire morphologyoptical, magnetic, and pseudocapacitance behavior of Co_3O_4, J. Phys. Chem. C 115 (2011) 25542–25556.
[39] D. Wang, Q. Wang, T. Wang, Morphology-controllable synthesis of cobalt oxalates and their conversion to mesoporous Co_3O_4 nanostructures for application in supercapacitors, Inorg. Chem. 50 (2011) 6482–6492.
[40] S. Xiong, C. Yuan, X. Zhang, B. Xi, Y. Qian, Controllable synthesis of mesoporous Co_3O_4 nanostructures with tunable morphology for application in supercapacitors, Chem. Eur. J. 15 (2009) 5320–5326.
[41] K. Mallikarjuna, H.-J. Hwang, W.-H. Chung, H.-S. Kim, Photonic welding of ultra-long copper nanowire network for flexible transparent electrodes using white flash light sintering, RSC Adv. 6 (2016) 4770–4779.
[42] J. Zhu, J. Jiang, Z. Sun, J. Luo, Z. Fan, X. Huang, H. Zhang, T. Yu, 3D carbon/cobalt-nickel mixed-oxide hybrid nanostructured arrays for asymmetric supercapacitors, Small 10 (2014) 2937–2945.
[43] Z. Fan, J. Yan, T. Wei, L. Zhi, G. Ning, T. Li, F. Wei, Asymmetric supercapacitors based on graphene/MnO_2 and activated carbon nanofiber electrodes with high power and energy density, Adv. Funct. Mater. 21 (2011) 2366–2375.
[44] P. Simon, Y. Gogotsi, B. Dunn, Where do batteries end and supercapacitors begin? Science 343 (2014) 1210–1211.
[45] K. Jang, S. Yu, S.-H. Park, H.-S. Kim, H. Ahn, Intense pulsed light-assisted facile and agile fabrication of cobalt oxide/nickel cobaltite nanoflakes on nickel-foam for high performance supercapacitor applications, J. Alloys Compd. 618 (2015) 227–232.
[46] B.V. L'vov, Mechanism of carbothermal reduction of ironcobalt, nickel and copper oxides, Thermochim. Acta 360 (2000) 109–120.
[47] I.G. Casella, M. Gatta, Study of the electrochemical deposition and properties of cobalt oxide species in citrate alkaline solutions, J. Electroanal. Chem. 534 (2002) 31–38.
[48] C. Barbero, G.A. Planes, M.C. Miras, Redox coupled ion exchange in cobalt oxide films, Electrochem. Commun. 3 (2001) 113–116.
[49] W. Liu, X. Li, M. Zhu, X. He, High-performance all-solid state asymmetric supercapacitor based on Co_3O_4 nanowires and carbon aerogel, J. Power Sources 282 (2015) 179–186.
[50] W.K. Behl, J.E. Toni, Anodic oxidation of cobalt in potassium hydroxide electrolytes, J. Electrochem. Soc. 31 (1971) 63–75.
[51] M. Jing, Y. Yang, Y. Zhu, H. Hou, Z. Wu, X. Ji, An asymmetric ultracapacitors utilizing α-$Co(OH)_2$/Co_3O_4 flakes assisted by electrochemically alternating voltage, Electrochim. Acta 141 (2014) 234–240.
[52] R. Vellacheri, A. Al-Haddad, H. Zhao, W. Wang, C. Wang, Y. Lei, High performance supercapacitor for efficient energy storage under extreme environmental temperatures, Nano Energy 8 (2014) 231–237.
[53] B. Vidyaharan, R.A. Aziz, I.I. Misnon, G.M. Anil Kumar, J. Ismail, M.M. Yusoff, R. Jose, High energy and power density asymmetric supercapacitors using electrospun cobalt oxide nanowire anode, J. Power Sources 270 (2014) 526–535.
[54] C. Tang, X. Yin, H. Gong, Superior performance asymmetric supercapacitors based on a directly grown commercial mass 3D Co_3O_4@$Ni(OH)_2$ core-shell electrode, ACS Appl. Mater. Interfaces 5 (2013) 10574–10582.
[55] Y. Jiang, L. Chen, H. Zhang, Q. Zhang, W. Chen, J. Zhu, D. Song, Two-dimensional Co_3O_4 thin sheets assembled by 3D interconnected nanoflake array framework structures with enhanced supercapacitor performance derived from coordination complexes, Chem. Eng. J. 292 (2016) 1–12.
[56] M. Pang, G. Long, S. Jiang, Y. Ji, W. Han, B. Wang, X. Liu, Y. Xi, D. Wang, F. Xu, Ethanol-assisted solvothermal synthesis of porous nanostructured cobalt oxides (CoO/Co_3O_4) for high-performance supercapacitors, Chem. Eng. J. 280 (2015) 377–384.
[57] R.R. Salunkhe, J. Tang, Y. Kamachi, T. Nakato, J.H. Kim, Y. Yamauchi, Asymmetric supercapacitors using 3D nanoporous carbon and cobalt oxide electrodes synthesized from a single metal-organic framework, ACS Nano 9 (2015) 6288–6296.
[58] M. Huang, Y. Zhang, F. Li, L. Zhang, Z. Wen, Q. Liu, Facile synthesis of hierarchical Co_3O_4@MnO_2 core-shell arrays on Ni foam for asymmetric supercapacitors, J. Power Sources 252 (2014) 98–106.